

New coercivities and Curie temperatures emerged in van der Waals homostructures of Fe_3GeTe_2

Shanchuan Liang ¹, Jierui Liang ¹, Jimmy C. Kotsakidis ², Hasitha Suriya Arachchige,³
David Mandrus,³ Adam L. Friedman ² and Cheng Gong ^{1,*}

¹*Department of Electrical and Computer Engineering and Quantum Technology Center, University of Maryland, College Park, Maryland 20742, USA*

²*Laboratory for Physical Sciences, College Park, Maryland 20740, USA*

³*Department of Materials Science and Engineering, The University of Tennessee, Knoxville, Tennessee 37996, USA*



(Received 4 July 2022; revised 5 May 2023; accepted 19 May 2023; published 7 June 2023)

Stacking of two-dimensional van der Waals (vdW) materials has emerged as a vital approach for investigating the complex interplay between coexisting materials, leading to novel electronic, photonic, and spintronic phenomena such as strong electronic correlation, enhanced Zeeman splitting of excitons, and the magnetic proximity effect. While most of the previous focus was on the electronic and photonic properties of vdW hetero-/homostructures, the study of magnetism in hetero-/homostructures remains lacking, though phenomena such as layer-dependent magnetism already highlighted the critical role of interlayer coupling in magnetism of layered systems. Here, we report an interesting two-step magnetic hysteresis loop in the homostructure of the layered vdW magnet Fe_3GeTe_2 (FGT). The two coercivities in the homostructure differ from that of each constituent FGT layer, indicating that the two constituents interact mutually but do not merge into a thicker uniform material. The Curie temperature (T_C) of the homostructure is in between that of the thinner and thicker constituents, further implying that the two constituent layers interact yet without forming a naturally occurring thicker layer. Our results highlight the unexplored opportunities that the rich interplay within vdW magnet homostructures can be employed to create emerging magnetic properties and develop novel multistate devices.

DOI: [10.1103/PhysRevMaterials.7.L061001](https://doi.org/10.1103/PhysRevMaterials.7.L061001)

I. INTRODUCTION

Layered van der Waals (vdW) materials [1–3] possess numerous possibilities for hetero/homostructure integrations that construct unique platforms for investigating the rich low-dimensional physics [4–8] that has been inaccessible in naturally occurring crystals. It has been well known that the properties of layered vdW materials are highly sensitive to the stacking order, twisting angle, and relative registry [9–11]. Since the discovery of correlated insulating states and superconductivity in the twisted bilayer and trilayer graphene [12–15], the exploration of moiré superlattices with flat band physics has achieved remarkable progress, both theoretically and experimentally. Regarding the recently discovered layered magnets [3,16–20], the interlayer exchange interaction was found to dictate the resultant magnetic configurations [21–25]. The notable examples include the skyrmions in vdW heterostructures of two-dimensional (2D) magnets that appear rooted in moiré-dependent interlayer magnetic coupling [26,27], and coexisting ferromagnetic and antiferromagnetic ground states were claimed by the competing interlayer interactions in the twisted homostructure of bilayer CrI_3 [28]. Nevertheless, the most fundamental physics properties of homostructured 2D magnets such as coercivity and Curie temperature (T_C) have remained elusive to date.

In this letter, by bringing together two few-layer Fe_3GeTe_2 (FGT) flakes, we investigated the new magnetic properties emerging in the FGT homostructure. Through reflectance magnetic circular dichroism (RMCD) studies, we observed a distinctive two-step magnetic hysteresis loop [29] in the FGT homostructure. The two coercive fields (H_C) (i.e., the two-step magnetic hysteresis loop has two H_C) of the FGT homostructure differ from that of each constituent FGT, strongly implying that the two component layers interact mutually but do not combine to form a uniform thicker FGT. Furthermore, our FGT homostructure has a T_C value of 188 K, which surprisingly lies in between, but not higher than, the thinner (175 K) and thicker (208 K) layers of the constituent FGT flakes. These interesting behaviors of the coercivity and T_C of the FGT homostructure in comparison to the two constituent FGT flakes alone indicate the significant role of the cross-layer interaction between the stacked FGT layers in the emergence of homostructures' new magnetic properties. These findings highlight the promising potential of developing 2D magnet homostructures for emerging properties and multistate spintronics [30].

II. METHODS

Sample preparation. The bulk Fe_3GeTe_2 single crystals were synthesized by the chemical vapor transport method. Atomically thin Fe_3GeTe_2 flakes were mechanically exfoliated from the as-synthesized crystals. The bottom Fe_3GeTe_2

*Corresponding author: gongc@umd.edu

was first exfoliated on polydimethylsiloxane (PDMS) and then transferred onto the 260-nm-thick SiO_2/Si substrate. Next, the top Fe_3GeTe_2 was exfoliated on PDMS in the same way and transferred to cover a part of the prepared bottom FGT on the 260-nm-thick SiO_2/Si substrate using the all-dry viscoelastic stamping procedure. The thicknesses of exfoliated 2D Fe_3GeTe_2 samples were identified by atomic force microscopy (AFM) after all measurements. The samples were stored in a glove box with oxygen and moisture levels below 0.1 ppm to prevent surface oxidation.

RMCD characterization. Our RMCD setup characterizes magnetic materials with out-of-plane magnetization via magnetic circular dichroism (MCD). When linearly polarized light [i.e., an equal mix of left circularly polarized light (LCP) and right circularly polarized light (RCP)] reflects off from the magnetic materials, the linear polarization becomes elliptically polarized due to the differential reflectance of LCP and RCP by the magnetic materials. The detailed RMCD setup is illustrated in Fig. S1 in the Supplementary Material [31]. In brief, RMCD characterization was conducted in a Montana closed-cycle cryostat down to 4 K under the out-of-plane magnetic field up to 300 mT. A He-Ne laser (633 nm) served as the excitation beam, with its intensity and helicity (i.e., LCP and RCP) modulated by a chopper and a photoelastic modulator (PEM), respectively. The excitation beam was focused onto a micrometer-size spot of the sample (laser power $\sim 7 \mu\text{W}$ at the sample surface) via a $50\times$ objective with a 0.5 numerical aperture. The reflected beam was collected by the same objective, separated from the incidence path via a beam-splitter filter, and detected by a photodiode. The signal collected by the photodiode was then sent into two lock-in amplifiers: one was set at the PEM frequency (50 kHz) to collect the AC signal for calculating the intensity difference between the reflected RCP and LCP (ΔR), and the other was tuned at the chopper frequency (237 Hz) to obtain the reflected light intensity (R_0). The RMCD is determined by $\Delta R/R_0$.

III. EXPERIMENTAL RESULTS

Figure 1(a) shows the schematic of the FGT homostructure experimentally prepared by stacking the bottom and top FGT layers. FGT is an itinerant vdW ferromagnet [34,35]. In the FGT monolayer, Fe_3Ge is covalently bonded as a heterometallic slab sandwiched between two Te layers [Fig. 1(b)]. Because of the reduced crystal symmetry and sizable spin-orbit coupling, strong out-of-plane magnetocrystalline anisotropy is generated in FGT. Such anisotropy is expected to stabilize the ferromagnetism in 2D FGT that can be well probed by our RMCD measurements (setup details shown in Fig. S1 in the Supplementary Material [31]). In this work, the bottom few-layer FGT flake was first exfoliated on PDMS and then transferred onto a 260-nm-thick- SiO_2/Si substrate. The top FGT flake was then exfoliated by the same method and transferred to cover a part of the bottom FGT on the SiO_2/Si substrate using the all-dry viscoelastic stamping procedure [36]. As the optical image shows in Fig. 1(c), the sample was defined as three regions, including the constituent top FGT (F2), the constituent bottom FGT (F1), and the FGT homostructure (FC), respectively. In the fabrication process,

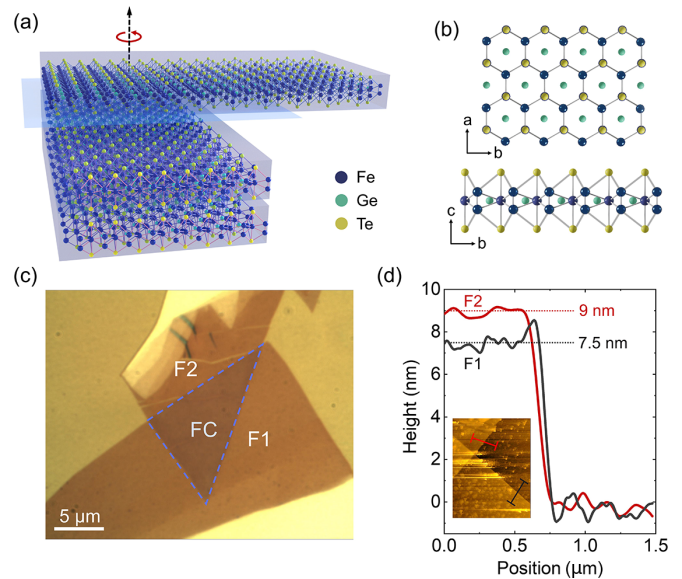


FIG. 1. Characterizations of the fabricated FGT homostructure. (a) Schematic of an FGT homostructure. The blue plane indicates the interface between two constituent FGT flakes. (b) Top and side views of the atomistic configuration of a supercell of monolayer FGT. (c) Optical image of the fabricated FGT homostructure (scale bar, $5 \mu\text{m}$). The blue dashed line defines the region of the FGT homostructure (indicated by the capital “FC” standing for “flakes combined”). F1 (standing for “flake 1”) and F2 (standing for “flake 2”) represent the bottom- and top-constituent FGT flakes, respectively. (d) Atomic force microscopy (AFM) line profiles of the two constituent FGT flakes (F1, black; F2, red). Inset shows the AFM image and the line scan positions (black and red lines). Note that the moisture/air gap between the exfoliated 2D flake and SiO_2 substrate [32] may cause the measured FGT step heights to be larger than the actual height, as observed with many other 2D materials [33].

top and bottom few-layer FGT flakes of different thicknesses were selected, which were first estimated by the optical contrast and were quantitatively identified by AFM measurements [Fig. 1(d)] afterwards.

To study the out-of-plane magnetization in the FGT homostructure, we first measured the RMCD while sweeping the external magnetic field applied perpendicular to the sample plane. The 633-nm HeNe laser employed for the RMCD measurements can be focused into a micrometer-size spot size, allowing us to select distinct locations (i.e., F1, F2, FC) of the sample for magnetization probing [Figs. 2(a)–2(h)]. Our laser spot was focused on the center of each region, which was away from the FGT-FGT stacked edges to avoid any potential edge complexities [37]. As shown in Figs. 2(e)–2(h), the ferromagnetic hysteresis loops were measured in both constituent FGT flakes (F1 and F2) at temperatures ranging from 140 to 110 K (well below the T_C of bulk FGT [35]). With the stronger thermal fluctuations at elevated temperatures, the H_C at 140 K gradually decreased in comparison to that at 130, 120, and 110 K. In stark contrast to the two constituent FGT flakes which have the conventional square-shaped hysteresis loops, the FGT homostructure shows distinct two-step hysteresis loops with two intermediate magnetic states at a broad temperature range [Figs. 2(a)–2(d)].

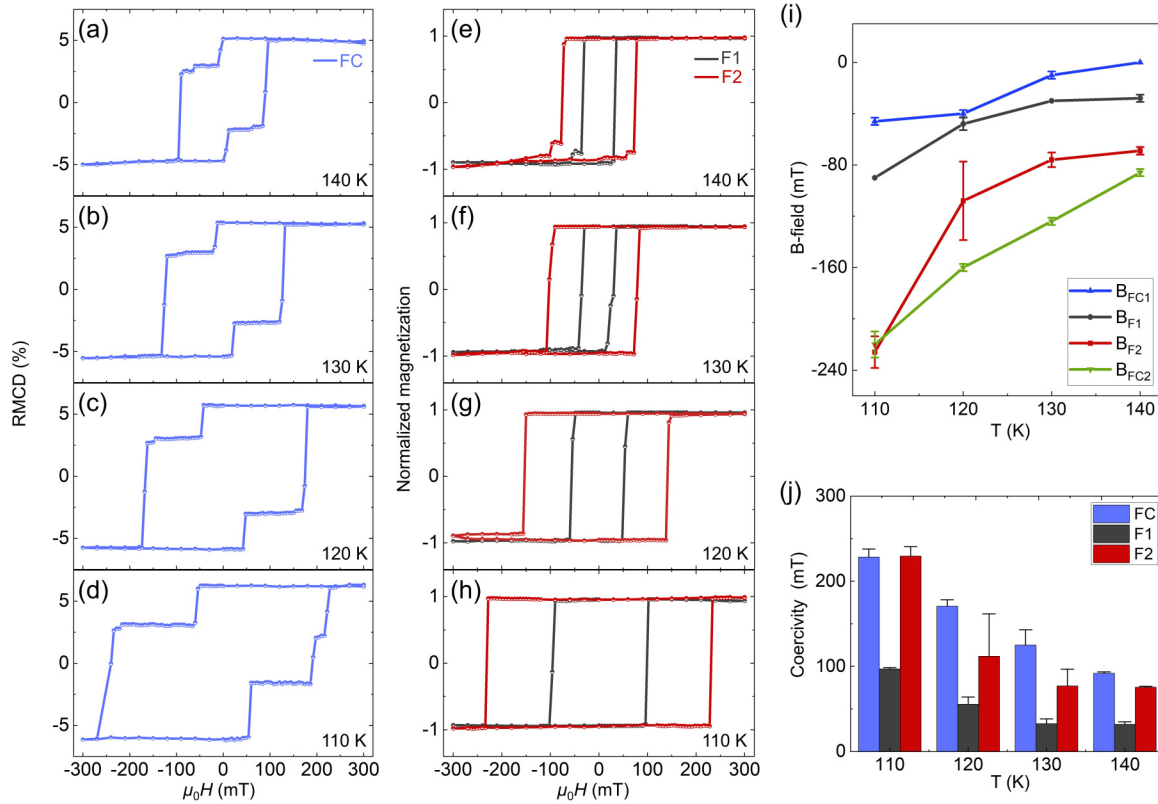


FIG. 2. RMCD measurements of an FGT homostructure. (a)–(d) Distinct two-step magnetic hysteresis loops of an FGT homostructure measured at different temperatures ranging from 140 to 110 K. (e)–(h) Standard square-shaped hysteresis loops obtained at two constituent FGT flakes F1 and F2 at different temperatures ranging from 140 to 110 K. The comparison between the results in (a)–(d) and those in (e)–(h) clearly shows that new magnetic states emerge in the homostructure. Interestingly, the two H_C values of the FGT homostructure differ from that of each constituent FGT flake owing to interflake interactions that alter both constituent layers. (i) Extracted critical B fields that switch the magnetization in F1, F2, and FC plotted against temperatures ranging from 140 to 110 K. The blue and green colors indicate the two B fields that cause the transition of spin orientation from all-spin-up to intermediate (B_{FC1}) and from intermediate to all-spin-down (B_{FC2}), respectively, in the FGT homostructure. The black (B_{F1}) and red (B_{F2}) indicate the B fields that cause the transition from all-spin-up to all-spin-down in the two constituent FGT flakes. The B_{FC1} and B_{FC2} differ from the B_{F1} and B_{F2} , suggesting the two constituent flakes interact mutually. (j) Extracted H_C in F1, F2, and FC with the temperature ranging from 140 to 110 K. Note the H_C in FC indicates the overall coercive field ignoring the intermediate state [i.e., B_{FC2} in (i)]. The trend shows the FC as the thickest region has the largest H_C at all temperatures. All error bars represent the standard deviations and are smaller than the plotted points if not shown.

In the homostructure, the two coercivities differ from that of each constituent FGT (F1 and F2), showing that the two component layers interact with one another at the interface but do not behave as a thicker uniform flake.

We also summarized the applied magnetic fields (B fields) corresponding to the coercivities in F1, F2, and FC in Fig. 2(i). Regarding the two coercivities associated with the altered magnetic properties in the FGT homostructure, the blue and green lines (Fig. 2(i), from 140 to 110 K) show the applied magnetic fields under which the switching between the magnetic states (i.e., from all-spin-up to the intermediate states and from the intermediate to all-spin-down states, respectively) start to occur. Similarly, in the constituent FGT flakes (F1 and F2), the summarized applied magnetic fields are only corresponding to where spin orientation is fully reversed (i.e., between all-spin-up and all-spin-down states, as reflected in a single-step hysteresis loop). It was clear that the two H_C values in the FGT homostructure differ from that of each constituent FGT layer, shown as the black (F1) and red (F2) dots in between the blue and green (FC region) dots in Fig. 2(i).

Specifically, the two H_C in the FGT homostructure are -12 and -90 mT at 140 K, whereas the H_C in the two constituent FGT flakes (F1 and F2) are -30 mT and -66 mT, respectively. Note that all this analysis is based on the backward sweep of the magnetic field (from 300 mT to -300 mT), and vice versa in the forward sweep owing to the symmetry of the hysteresis loop. The coercivity difference between the FGT homostructure and the constituent FGT layers is direct evidence highlighting that the interaction between the adjacent FGT layers alters the magnetic properties of each other, leading to the altered properties of the FGT homostructure, but meanwhile, the interaction between the constituent FGT layers is not strong enough to merge them into a uniform thicker layer (which would otherwise exhibit only one coercivity in a single-step hysteresis).

To directly visualize the multiple magnetic states of the FGT homostructure, we conducted an RMCD mapping of the entire sample including F1, F2, and FC (indicated by the annotations in Fig. 3) at 120 K. The spin orientation of the magnetic domain in FGT was initially aligned in the

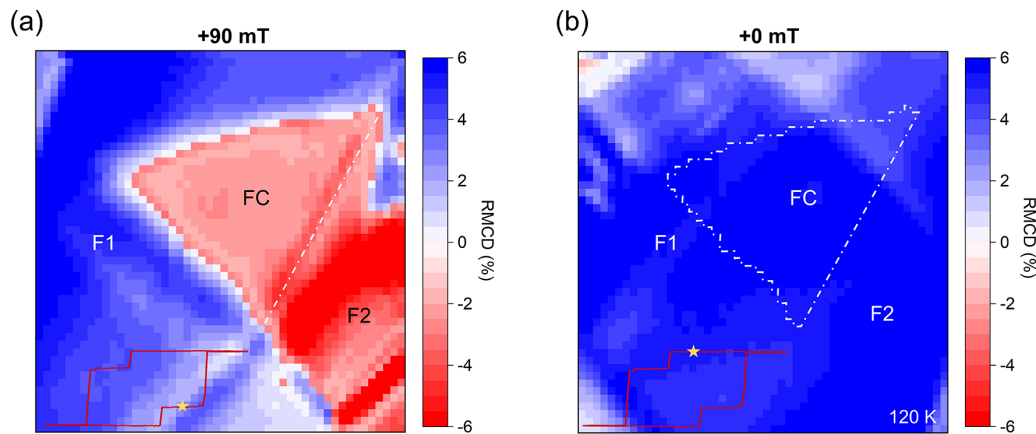


FIG. 3. RMCD mapping of the FGT homostructure. (a) RMCD mapping of the entire sample after the external magnetic field was swept from -300 mT (when the whole sample is magnetized to the spin-down configuration) to 90 mT (when the F2 remains spin-down but the F1 is flipped to spin-up and FC is flipped to an intermediate state). The pink domain (FC) in (a) indicates the intermediate magnetic state that appeared between all-spin-up (blue) and all-spin-down (red) orientations. (b) RMCD mapping of the entire sample after the external magnetic field was swept from 300 mT (when the whole sample is magnetized to the spin-up configuration) to 0 mT (when all F1, F2, and FC remain in the spin-up configuration). Insets represent the positions of the applied B fields in the full hysteresis loop. The color bar is plotted by the RMCD value, indicating the spin-up (blue) and spin-down (red) domains.

all-spin-down direction by applying the external magnetic field of -300 mT. The RMCD mapping was then scanned after sweeping the magnetic field to 90 mT (the position of this applied field in the hysteresis loop of the FGT homostructure is indicated in Fig. 3(a) inset), which can flip the magnetic domains in F1 to all-spin-up and that in FC to the intermediate state but remain insufficient to flip the all-spin-down domains in F2. As shown in Fig. 3(a), while the domain orientation in F2 remains spin-down (red for spin-down and blue for spin-up), the spins in F1 are flipped to the all-spin-up and the spins in FC appear between the spin-up and spin-down (shown as the pink area). The RMCD value difference among the three regions (i.e., roughly -6 in F2, 2 in FC, and 6 in F1) also agrees well with the result in the magnetic hysteresis loop in Fig. 2(c), indicating clearly the emergence of an intermediate magnetic state. In another measurement, the RMCD mapping was scanned after the magnetic field was swept from 300 to 0 mT (illustrated in Fig. 3(b) inset), and all three regions in Fig. 3(b) remained in the all-spin-up orientation in stark contrast to the results with multiple magnetic states shown in Fig. 3(a). These RMCD mappings visualize the existence of multiple magnetic states in the FGT homostructure, which is controllable by applying different external magnetic fields, promising the future multistate spintronics.

The two-step hysteresis loops with coercivities differing from constituent layers unravel the interflake effects on the resultant magnetic anisotropies of the FGT homostructure, while studying the T_C of the FGT homostructure can reveal more about the interflake effect on the exchange interaction in the FGT homostructure. Intuitively, the ferromagnetic order in the three regions should disappear above their respective T_C in the sequence of F1, F2, and FC, because of their increasing thicknesses. However, our experiments show a difference from this simple intuition. Figures 4(a)–4(c) show the magnetic hysteresis loops of FC, F1, and F2 obtained by RMCD at an elevated temperature of 165 K when the ferromagnetic order is weakened due to thermal fluctuations.

Regarding the two constituent FGT layers, the hysteresis loop of F1 almost vanishes because the temperature approaches its T_C [Fig. 4(b)], whereas the hysteresis remains obvious in F2 [Fig. 4(c)]. Remarkably, the coercivity of FC lies in between the respective coercivities of F1 and F2, which would otherwise be the largest according to the simple intuition that the thickest FC should have the highest T_C and the largest coercivity at elevated temperatures. Additionally, the FC region no longer behaves in the two-step hysteresis loop as it does at lower temperatures. Indeed, at 155 K, the two-step hysteresis loop in the FC region has already disappeared, and the coercivity of FC becomes smaller than that of F2 (Fig. S2 in the Supplementary Material [31]). These findings suggest that, despite the FGT homostructure being the thickest of the three regions, its T_C is not the highest, implying that the two constituent layers interact but do not merge into a naturally occurring thicker layer.

To precisely determine the T_C values of different regions, we conducted the temperature-dependent RMCD at different regions (FC, F1, and F2). The RMCD values were recorded at various temperatures during the warming-up procedure with a small magnetic field ($+6$ mT) applied. As shown in Fig. 4(d), the FGT homostructure that is the thickest has a T_C value of 188 K which lies in between the respective T_C values of the two constituent FGT flakes (i.e., the thinner part F1 has a T_C of 175 K and the thicker flake F2 has a T_C of 208 K), contradicting the simple intuition that T_C increases monotonically with the increasing thickness of vdW layered magnets [34,35]. To help understand the anomalous T_C in the FGT homostructure, we summarize a probable scenario of magnetic phases of F1, F2, and FC regions at 180 K in Fig. 4(e) when the temperature is slightly above the T_C of F1 (i.e., 175 K). Specifically, when F1 enters the paramagnetic phase at above 175 K, the paramagnetic F1 in the homostructure may weaken the exchange interaction/magnetic anisotropy in the adjacent F2 in the homostructure, leading to the reduced T_C of F2 in the homostructure (i.e., 188 K) with respect

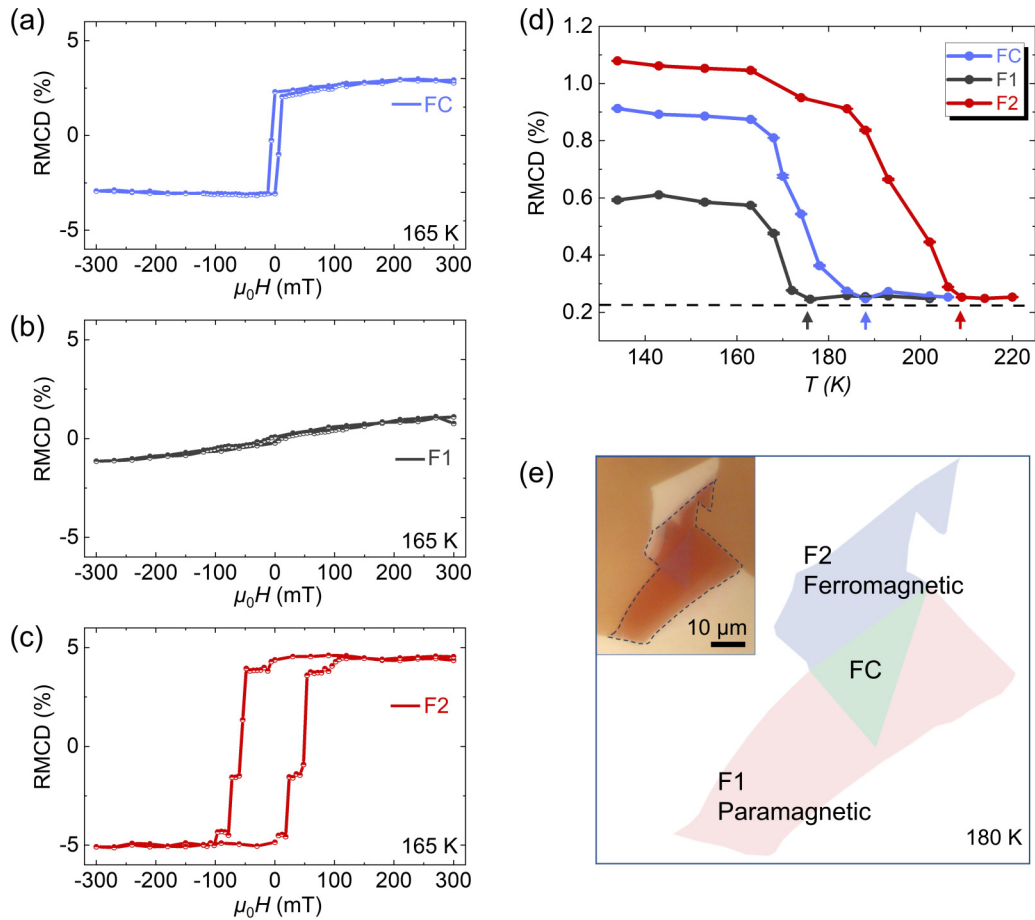


FIG. 4. Examining the anomalous T_C of the FGT homostructure. (a)–(c) Magnetic hysteresis loops obtained at an elevated temperature of 165 K in FC (in ferromagnetic phase, but no longer exhibiting the two-step hysteresis loop), F1 (almost entering the paramagnetic phase), and F2 (ferromagnetic phase). (d) RMCD as a function of temperature obtained from FC, F1, and F2 in the sample. Arrows mark the ferromagnetic transition temperatures T_C and the vertical error bars on all dots represent the standard deviations of RMCD values. The sample was first cooled down to 130 K under zero field, and then the RMCD values were recorded during the heating process under the out-of-plane magnetic field of +6 mT. The T_C of the FGT homostructure FC sits in between the two constituent FGT parts F1 and F2. (e) Illustration of the magnetic phases of different regions of the sample at 180 K (i.e., slightly above the T_C of F1). The inset is the optical image of the sample (scale bar, 10 μm).

to the standing alone F2 flake (i.e., 208 K). Note that in 2D vdW layered magnets, both magnetic anisotropy and exchange interaction play significant roles in determining the T_C [3]. In our FGT homostructure, the magnetic anisotropy of one constituent FGT flake in the FC region can be influenced by interfacing with another FGT flake and vice versa. Additionally, the electronic redistribution can occur at the interface, affecting the exchange interaction within each of the two constituent FGT flakes in the FC region. A further quantitative analysis to disentangle these factors would require extensive interfacial details and theoretical calculations, which is beyond the scope of this work. Nevertheless, the observed unusual T_C of the FGT homostructure clearly indicates that both the exchange interaction and magnetic anisotropy of each constituent layer are altered when forming the FGT homostructure.

In conclusion, we fabricated an FGT vdW homostructure and observed distinct two-step hysteresis loops with multiple magnetic states. Especially, the two coercivities in the homostructure differ from that of each constituent, featured by the presence of two stable intermediate magnetic states.

Moreover, we discovered an anomalous T_C in the FGT homostructure in comparison with the two constituent FGT flakes that made up the homostructure. Our findings indicate that both the magnetic anisotropy and exchange interaction of each of the constituent layers are altered when they form a homostructure. These observations suggest the two constituent layers interact mutually but do not merge into a thicker uniform FGT. Our observations provide fundamental insights into FGT homostructures and a pathway toward multistate spintronic devices. We note that the subtle dependence of the emergent magnetic states on layer thickness, twisting angle, and relative registry are interesting scientific questions that would require an extensive amount of future work to fully understand and thus are beyond the scope of this work.

ACKNOWLEDGMENTS

C.G. acknowledges the grant support from Air Force Office of Scientific Research under Award No. FA9550-22-1-0349, Naval Air Warfare Center Aircraft Division under Award

No. N00421-22-1-0001, Army Research Laboratory Cooperative Agreement No. W911NF-19-2-0181, and National

Science Foundation under Award No. CMMI-2233592 and No. 49100423C0011.

- [1] K. S. Novoselov, D. Jiang, F. Schedin, T. J. Booth, V. V. Khotkevich, S. V. Morozov, and A. K. Geim, *Proc. Natl. Acad. Sci.* **102**, 10451 (2005).
- [2] S. Manzeli, D. Ovchinnikov, D. Pasquier, O. V. Yazyev, and A. Kis, *Nat. Rev. Mater.* **2**, 17033 (2017).
- [3] C. Gong and X. Zhang, *Science* **363**, eaav4450 (2019).
- [4] C. R. Dean, A. F. Young, I. Meric, C. Lee, L. Wang, S. Sorgenfrei, K. Watanabe, T. Taniguchi, P. Kim, K. L. Shepard, and J. Hone, *Nat. Nanotechnol.* **5**, 722 (2010).
- [5] F. Withers, O. Del Pozo-Zamudio, A. Mishchenko, A. P. Rooney, A. Gholinia, K. Watanabe, T. Taniguchi, S. J. Haigh, A. K. Geim, A. I. Tartakovskii, and K. S. Novoselov, *Nat. Mater.* **14**, 301 (2015).
- [6] Y. Liu, N. O. Weiss, X. Duan, H.-C. Cheng, Y. Huang, and X. Duan, *Nat. Rev. Mater.* **1**, 16042 (2016).
- [7] K. S. Novoselov, A. Mishchenko, A. Carvalho, and A. H. Castro Neto, *Science* **353**, aac9439 (2016).
- [8] D. Zhong, K. L. Seyler, X. Linpeng, R. Cheng, N. Sivadas, B. Huang, E. Schmidgall, T. Taniguchi, K. Watanabe, M. A. McGuire, W. Yao, D. Xiao, K.-M. C. Fu, and X. Xu, *Sci. Adv.* **3**, e1603113 (2017).
- [9] R. Ribeiro-Palau, C. Zhang, K. Watanabe, T. Taniguchi, J. Hone, and C. R. Dean, *Science* **361**, 690 (2018).
- [10] Y. Cao, V. Fatemi, A. Demir, S. Fang, S. L. Tomarken, J. Y. Luo, J. D. Sanchez-Yamagishi, K. Watanabe, T. Taniguchi, E. Kaxiras, R. C. Ashoori, and P. Jarillo-Herrero, *Nature (London)* **556**, 80 (2018).
- [11] W. Chen, Z. Sun, Z. Wang, L. Gu, X. Xu, S. Wu, and C. Gao, *Science* **366**, 983 (2019).
- [12] Y. Cao, V. Fatemi, S. Fang, K. Watanabe, T. Taniguchi, E. Kaxiras, and P. Jarillo-Herrero, *Nature (London)* **556**, 43 (2018).
- [13] Z. Zhu, S. Carr, D. Massatt, M. Luskin, and E. Kaxiras, *Phys. Rev. Lett.* **125**, 116404 (2020).
- [14] C. Mora, N. Regnault, and B. A. Bernevig, *Phys. Rev. Lett.* **123**, 026402 (2019).
- [15] Z. Zhu, P. Cazeaux, M. Luskin, and E. Kaxiras, *Phys. Rev. B* **101**, 224107 (2020).
- [16] C. Gong, L. Li, Z. Li, H. Ji, A. Stern, Y. Xia, T. Cao, W. Bao, C. Wang, Y. Wang, Z. Q. Qiu, R. J. Cava, S. G. Louie, J. Xia, and X. Zhang, *Nature (London)* **546**, 265 (2017).
- [17] B. Huang, G. Clark, E. Navarro-Moratalla, D. R. Klein, R. Cheng, K. L. Seyler, D. Zhong, E. Schmidgall, M. A. McGuire, D. H. Cobden, W. Yao, D. Xiao, P. Jarillo-Herrero, and X. Xu, *Nature (London)* **546**, 270 (2017).
- [18] K. S. Burch, D. Mandrus, and J.-G. Park, *Nature (London)* **563**, 47 (2018).
- [19] M. Gibertini, M. Koperski, A. F. Morpurgo, and K. S. Novoselov, *Nat. Nanotechnol.* **14**, 408 (2019).
- [20] S. Liang, T. Xie, N. A. Blumenschein, T. Zhou, T. Ersevrim, Z. Song, J. Liang, M. A. Susner, B. S. Conner, S.-J. Gong, J.-P. Wang, M. Ouyang, I. Žutić, A. L. Friedman, X. Zhang, and C. Gong, *Nat. Electron.* **6**, 199 (2023).
- [21] N. Sivadas, S. Okamoto, X. Xu, C. J. Fennie, and D. Xiao, *Nano Lett.* **18**, 7658 (2018).
- [22] P. Jiang, C. Wang, D. Chen, Z. Zhong, Z. Yuan, Z.-Y. Lu, and W. Ji, *Phys. Rev. B* **99**, 144401 (2019).
- [23] D. Soriano, C. Cardoso, and J. Fernández-Rossier, *Solid State Commun.* **299**, 113662 (2019).
- [24] T. Li, S. Jiang, N. Sivadas, Z. Wang, Y. Xu, D. Weber, J. E. Goldberger, K. Watanabe, T. Taniguchi, C. J. Fennie, K. Fai Mak, and J. Shan, *Nat. Mater.* **18**, 1303 (2019).
- [25] T. Song, Z. Fei, M. Yankowitz, Z. Lin, Q. Jiang, K. Hwangbo, Q. Zhang, B. Sun, T. Taniguchi, K. Watanabe, M. A. McGuire, D. Graf, T. Cao, J.-H. Chu, D. H. Cobden, C. R. Dean, D. Xiao, and X. Xu, *Nat. Mater.* **18**, 1298 (2019).
- [26] Q. Tong, F. Liu, J. Xiao, and W. Yao, *Nano Lett.* **18**, 7194 (2018).
- [27] M. Akram and O. Erten, *Phys. Rev. B* **103**, L140406 (2021).
- [28] Y. Xu, A. Ray, Y.-T. Shao, S. Jiang, K. Lee, D. Weber, J. E. Goldberger, K. Watanabe, T. Taniguchi, D. A. Muller, K. F. Mak, and J. Shan, *Nat. Nanotechnol.* **17**, 143 (2022).
- [29] Z. Tu, T. Zhou, T. Ersevrim, H. S. Arachchige, A. T. Hanbicki, A. L. Friedman, D. Mandrus, M. Ouyang, I. Žutić, and C. Gong, *Appl. Phys. Lett.* **120**, 043102 (2022).
- [30] C. Hu, D. Zhang, F. Yan, Y. Li, Q. Lv, W. Zhu, Z. Wei, K. Chang, and K. Wang, *Sci. Bull.* **65**, 1072 (2020).
- [31] See Supplemental Material at <http://link.aps.org/supplemental/10.1103/PhysRevMaterials.7.L061001> for comprehensive details on the optical setup for RMCD measurements in Fig. S1, and Magnetic field dependence of RMCD on FC, F1, and F2 at 155 K in Fig. S2.
- [32] P. Nemes-Incze, Z. Osváth, K. Kamarás, and L. P. Biró, *Carbon* **46**, 1435 (2008).
- [33] C. J. Shearer, A. D. Slattery, A. J. Stapleton, J. G. Shapter, and C. T. Gibson, *Nanotechnology* **27**, 125704 (2016).
- [34] Y. Deng, Y. Yu, Y. Song, J. Zhang, N. Z. Wang, Z. Sun, Y. Yi, Y. Z. Wu, S. Wu, J. Zhu, J. Wang, X. H. Chen, and Y. Zhang, *Nature (London)* **563**, 94 (2018).
- [35] Z. Fei, B. Huang, P. Malinowski, W. Wang, T. Song, J. Sanchez, W. Yao, D. Xiao, X. Zhu, A. F. May, W. Wu, D. H. Cobden, J.-H. Chu, and X. Xu, *Nat. Mater.* **17**, 778 (2018).
- [36] A. Castellanos-Gomez, M. Buscema, R. Molenaar, V. Singh, L. Janssen, H. S. J. van der Zant, and G. A. Steele, *2D Mater.* **1**, 011002 (2014).
- [37] Z. Cheng, H. Zhang, S. T. Le, H. Abuzaid, G. Li, L. Cao, A. V. Davydov, A. D. Franklin, and C. A. Richter, *ACS Nano* **16**, 5316 (2022).